

Saffman-Taylor problem in sector geometry: Solution and selection

Yuhai Tu

*Department of Physics and Institute for Nonlinear Science, University of California, San Diego
La Jolla, California 92093*

(Received 2 January 1991)

We develop an analytical method to extend the two-parameter family of analytical solutions in channel geometry to sector geometry with arbitrary opening angle at zero surface tension. We then show how to apply the WKB method to select the limiting finger width at very small surface tension. The result agrees very well with experiment. We also discuss stability of the pattern based on the special structure of these selected solutions.

I. INTRODUCTION

In recent years, patterns formed by the instabilities in propagating interfaces between different phases have received much attention [1]. One of the well-known examples is the Saffman-Taylor problem in a Hele-Shaw cell [2], where a unique finger pattern is observed when a viscous fluid is displaced by a less-viscous fluid.

The analytic theory of the determination of this finger shape is by now quite complete. The first step was taken by Saffman and Taylor in their original paper [3], where they found a family of analytical solutions parametrized by the width of the finger at zero surface tension. However, regular perturbation methods treating surface tension as a small perturbation did not reveal any evidence of selection. The puzzle was not solved until in studying some simple interface models it was realized that the surface tension cannot be treated perturbatively [4]. In fact, the presence of surface tension will generate exponentially small terms which destroy the interface smoothness at all but certain allowed widths $\{\lambda_i\}$. Numerically it was also seen that the continuous family of solutions breaks down to a set of discrete solutions [5]. Finally, matching the asymptotic behavior of the shape function in the complex plane, which actually takes the surface-tension-induced singularity into account, did indeed show the presence of this selection mechanism [6]. It was further shown numerically [7] and also analytically [8] using a WKB method that the finger with the smallest width is the only linear stable solution.

The same experiment was also done in different geometries [9], in particular, in a sector-shaped cell with arbitrary opening angle. It was observed that, just as in the linear geometry, at large velocity a unique finger tends to occupy a well-determined fraction of the cell angular width. This fraction is an increasing function of the opening angle that approaches 0.5 as the angle approaches 0° . The only theoretical attempt to explain the selected finger width in this type of geometry is by Brener, Kessler, Levine, and Rappel (BKLR) [10]. They applied the same WKB method used for the linear geometry to a family of analytic solutions found by Thome *et al.* [9] in the 90° cell. Their result of the select-

ed finger width at small surface tension agrees with experiment. The use of the WKB method (or any analytical method) is based on knowing the analytical zero-surface-tension solution. Until now no analytical solution has been found for any angle other than 90° .

In this paper, we develop a systematic method for deriving the zero-surface-tension solutions analytically at arbitrary opening angle. The solutions can be very easily extended to the complex plane. By using the WKB method, we can obtain the selected finger width at small surface tension. We also show that the structures of the selected solutions are different from that of the linear geometry due to the difference of the distribution of poles and branch cut for the phase integral. We further discuss the stability of the selected solutions within the WKB scheme based on the special structure of the solutions.

The outline of the paper is as follows. First, in Sec. II we will demonstrate our general method to obtain the two-parameter family of zero-surface-tension solutions. Then, in Sec. III we will apply the WKB method to the symmetric solutions for all opening angles and determine the selected finger width. We will also discuss the stability of the selected solutions. Finally, in Sec. IV we will summarize our results.

II. SOLUTIONS WITHOUT SURFACE TENSION

The evolution equations for the interface in the sector geometry are easy to derive [see Fig. 1(a)]. Inside the viscous fluid, the velocity potential ϕ satisfies the Laplace equation

$$\nabla^2\phi=0 \quad (1)$$

with the boundary conditions

$$\phi=\gamma\kappa|_{AOB}, \quad \left. \frac{\partial\phi}{\partial n} \right|_{AC(BD)}=0, \quad (2)$$

where γ is the surface-tension parameter and κ is the curvature of the interface. If the injection rate at infinity is normalized to 2π , ϕ has the behavior $\phi\sim(2\pi/\theta_0)\ln(x^2+y^2)^{1/2}$ as $x^2+y^2\rightarrow\infty$. The interface moves with the velocity

$$v_n = \mathbf{n} \cdot \nabla \phi|_{AOB} \quad (3)$$

We are interested in obtaining the zero-surface-tension solution in this section, so we set $\gamma = 0$.

Following Thome *et al.* [9], we consider the problem using the hodograph method, i.e., considering $z = x + iy$ as an analytical function of the complex velocity potential $\omega = \phi + i\psi$, with ψ the stream function. The interface equation of motion Eq. (3) is now

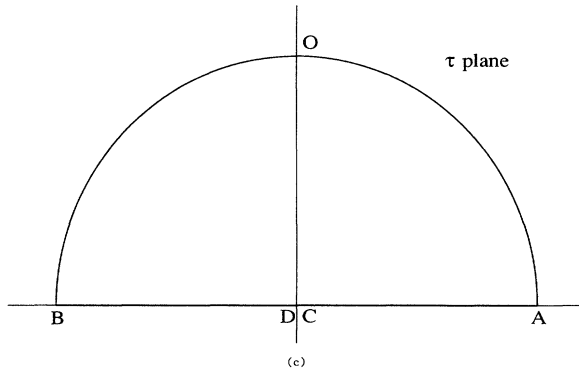
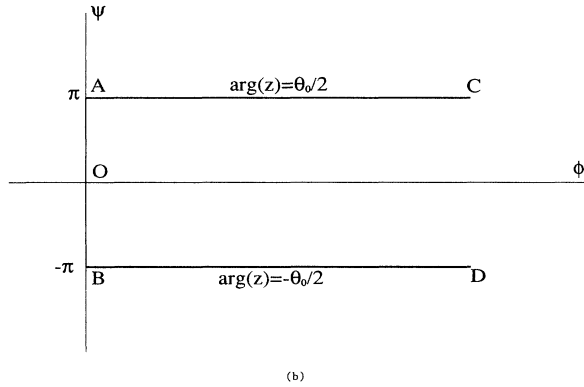
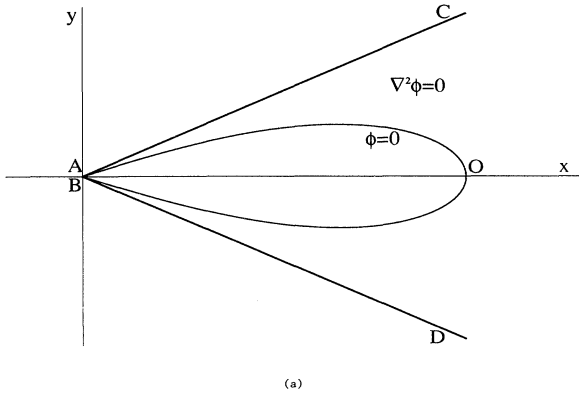


FIG. 1. Schematic picture of the Saffman-Taylor problem in sector geometry (AC and BD are the boundaries of the sector; AOB is the interface) in (a) physical space, (b) the ω plane, (c) the τ plane.

$$\frac{\partial x}{\partial t} \frac{\partial y}{\partial \psi} - \frac{\partial y}{\partial t} \frac{\partial x}{\partial \psi} = 1, \quad \psi = 0 \quad (4)$$

Because of the two-dimensional nature of the geometry, instead of looking for a solution translating with constant velocity as in the linear channel, we are seeking self-similar solutions here, written as

$$\begin{aligned} x(t, \phi=0, \psi) &= h(t)x(\psi), \\ y(t, \phi=0, \psi) &= h(t)y(\psi). \end{aligned} \quad (5)$$

Substituting this into Eq. (4), we have (superscript asterisk representing the complex conjugate)

$$\text{Im} \left[z^* \frac{\partial z}{\partial \psi} \right] = 1, \quad (6)$$

while $h(t)$ satisfies

$$h(t) \frac{dh(t)}{dt} = 1, \quad h(t) = \sqrt{2(t-t_0)}, \quad (7)$$

where t_0 is the initial time.

Thus the problem of finding the zero-surface-tension solutions reduces now to finding an analytical function z in the region $\phi \geq 0, -\pi < \psi < \pi$ [see Fig. 1(b)], satisfying the following three conditions as stated in Ref. 9: (i) $\arg(z) = \pm\theta_0/2$ on AC and BD , i.e., the half lines $\psi = \pm\pi$; (ii) $z \sim \exp(\omega\theta_0/2\pi)$ when $\phi \rightarrow \infty$; and (iii) z satisfies Eq. (6) on AOB , i.e., on $\phi = 0$.

Let us start by analyzing condition (iii) first. Differentiating both sides of Eq. (6) with respect to ψ , and because $(\partial z^*/\partial \psi)(\partial z/\partial \psi)$ is real, we obtain

$$\text{Im} \left[z^* \frac{\partial^2 z}{\partial \psi^2} \right] = 0, \quad \phi = 0, \quad (8)$$

so $\partial^2 z/\partial \psi^2$ should be equal to z times some real function of $\psi, f(\psi)$:

$$\frac{\partial^2 z}{\partial \psi^2} = f(\psi)z, \quad \phi = 0. \quad (9)$$

To interpolate the equation from $\phi = 0$ to the whole region, we can replace ψ by ω/i , and the equation becomes

$$\frac{-\partial^2 z}{\partial \omega^2} = f(-i\omega)z. \quad (10)$$

Next, we consider the second condition, namely, as $\omega \rightarrow \infty, z \sim e^{\theta_0\omega/2\pi}$. This determines the limiting behavior of $f(-i\omega)$: $f(-i\omega) \rightarrow -(\theta_0/2\pi)^2$ as $\omega \rightarrow \infty$. We subtract the constant part from $f(-i\omega)$ and define

$$f(-i\omega) \equiv -[(\theta_0/2\pi)^2 + f_1(\omega)]. \quad (11)$$

We also make the corresponding transformations for z :

$$z = \exp(\theta_0\omega/2\pi)z_1. \quad (12)$$

The equation for z_1 is then

$$\frac{d^2 z_1}{d\omega^2} + \frac{\theta_0}{\pi} \frac{dz_1}{d\omega} = f_1(\omega)z_1, \quad (13)$$

with the conditions for f_1 that $f_1(\omega) \rightarrow 0$ as $\omega \rightarrow \infty$ and

$f_1(\omega)$ must be real for pure-imaginary ω . For future convenience, we change the region of interest to a finite region by the transformation [see Fig. 1(c)]

$$\tau = [-\exp(\omega)]^{-1/2}. \quad (14)$$

The equation for z_1 changes to

$$\frac{d^2 z_1}{d\tau^2} + \frac{1-2\theta_0/\pi}{\tau} \frac{dz_1}{d\tau} = 4\tau^{-2} f_2(\tau) z_1, \quad (15)$$

where $f_2(\tau) = f_1(\ln(-\tau^{-2}))$. The conditions for f_2 are $f_2(\tau) \rightarrow 0$ as $\tau \rightarrow 0$ and $f_2(\tau)$ must be real on the unit circle, i.e., when $|\tau| = 1$.

Finally, we come to the last condition, which requires $\arg(z) = \pm\theta_0/2$ on $\psi = \pm\pi$. Because of the transformations (12) and (14), this condition now requires that the solution z_1 of Eq. (15) must be real on the real τ axis in the range $-1 \leq \tau \leq 1$.

Now the problem has been reduced to finding an analytic function $f_2(\tau)$ which satisfies all the above conditions, and then solving the linear ordinary differential Eq. (15) to obtain the mapping $z_1(\tau)$ from the τ plane [Fig. 1(c)] to real space [Fig. 1(a)].

We first consider the behavior of z_1 around the singular point $\tau=0$. Because $f_2(\tau) \rightarrow 0$ as $\tau \rightarrow 0$, the leading-order behavior is determined by the two terms at the left-hand side of Eq. (15). We can express the two solutions in power series around $\tau=0$:

$$\begin{aligned} z_1^{(1)} &= 1 + a_1 \tau + a_2 \tau^2 + \dots, \\ z_1^{(2)} &= \tau^{2\theta_0/\pi} (1 + b_1 \tau + b_2 \tau^2 + \dots), \end{aligned} \quad (16)$$

where a_i and b_i are constants, and the general solution is $z_1 = Az_1^{(1)} + Bz_1^{(2)}$ with A and B arbitrary constants. In order to satisfy the condition that z_1 be real on the real line segment $-1 \leq \tau \leq 1$, we must choose $B=0$ (except for the case $\theta_0 = \pi/2$, which will be discussed at the end of this section) and $f_2(\tau)$ has to be a real function of τ .

Other singular points of Eq. (15) will come from the poles of $f_2(\tau)$. Assume that $f_2(\tau)$ has a pole at $\tau = \tau_0$, then $z_1(\tau)$ will map τ_0 into $z_1 = 0$, which is on the interface, so τ_0 has to be on the semi-unit-circle $|\tau_0| = 1$. This is also required by the previous consideration, because if $z_1(\tau)$ has a singular point at some τ inside the unit circle, solution $z_1^{(1)}$ cannot be extended toward $\tau = \pm 1$. More strictly, because we are only interested in the physically meaningful case where the interface has only one bump, τ_0 has to be ± 1 . Generally, this problem allows more than one bump, accomplished by choosing $f_2(\tau)$ to have second-rank poles at points on the semi-unit-circle other than $\tau = \pm 1$. For example, if $f_2(\tau)$ generates a single bump solution in angle θ_0 , then function $f_2^{\text{new}}(\tau) = f_2(\tau^n)$ will generate an n -bump solution in angle $n\theta_0$. It is clear that $f_2^{\text{new}}(\tau)$ has $(n-1)$ other poles on the semi-unit-circle.

Let us analyze the local behavior of the mapping around $\tau = \pm 1$. Comparing the A corner in Figs. 1(a) and 1(c), we can see that the angle between the interface and the boundary wall changes in these two coordinate systems. So the mapping around $\tau = \pm 1$ should have the

form $z_1(\tau) \sim (\tau \mp 1)^{s_{\pm}}$, where $s_{\pm} (> 0)$ are constants that determine the relative angular width of the finger to the sector. Substituting this behavior into Eq. (15), we can easily see that $f_2(\tau)$ has two second rank poles at $\tau = \pm 1$.

Now we can finally gather all the properties of function $f_2(\tau)$ and determine its form. First, $f_2(\tau)$ is a real function of τ , and it also has to be real on the unit circle, so

$$f_2(e^{i\psi}) = [f_2(e^{i\psi})]^* = f_2^*(e^{-i\psi}) = f_2(e^{-i\psi}). \quad (17)$$

Interpolating to the whole region, we have

$$f_2(\tau) = f_2(1/\tau), \quad (18)$$

so the function $f_2(\tau)$ is constructed by two building blocks: $\tau + 1/\tau$ and $(\tau - 1/\tau)^2$. Remembering that $f_2(\tau)$ has second-rank poles at $\tau = \pm 1$ and $f_2(\tau) \rightarrow 0$ as $\tau \rightarrow 0$, we immediately have the general form $f_2(\tau)$:

$$f_2(\tau) = [c_1 + c_2(\tau + \tau^{-1})]/(\tau - \tau^{-1})^2, \quad (19)$$

where c_1 and c_2 are real constants. We make the following transformation:

$$c_1 = \frac{1}{4} [\frac{1}{2}(\lambda_1^2 + \lambda_2^2) - 1], \quad c_2 = \frac{1}{16} (\lambda_1^2 - \lambda_2^2). \quad (20)$$

The reason for this transformation will soon be clear. Substituting the expression of $f_2(\tau)$ into Eq. (15), we have

$$\begin{aligned} \frac{d^2 z_1}{d\tau^2} + \frac{1-2\theta_0/\pi}{\tau} \frac{dz_1}{d\tau} \\ = \frac{1}{\tau(\tau^2 - 1)^2} \left[\left[\frac{\lambda_1^2 + \lambda_2^2}{2} - 1 \right] \tau + \frac{\lambda_1^2 - \lambda_2^2}{4} (\tau^2 + 1) \right]. \end{aligned} \quad (21)$$

We have to choose the correct solution to this equation: the $z_1^{(1)}(\tau)$ that has finite derivatives to any order at $\tau = 0$.

Let us check the behavior of $z_1(\tau)$ around $\tau = \pm 1$. At the neighborhood of $\tau = 1$, the leading-order behavior of $z_1(\tau)$ is $(1-\tau)^{(1-\lambda_1)/2}$ (assuming $\lambda_{1(2)} \geq 0$). In order that $z_1(1) = 0$, we have $0 \leq \lambda_1 \leq 1$; the same condition also applies for λ_2 . Solving the linear ordinary differential Eq. (21), we obtain a two-parameter family of solutions parametrized by λ_1 and λ_2 , analogous to the two-parameter Saffman-Taylor solutions found in the linear channel. The solutions with $\lambda_1 \neq \lambda_2$ will give asymmetric interfaces, while the solutions with $\lambda_1 = \lambda_2$ correspond to symmetric interfaces. The effective angular width λ_{eff} of the finger with respect to the opening angle of the sector can be expressed as

$$\lambda_{\text{eff}} = 1 - \frac{\pi}{2\theta_0} [1 - \frac{1}{2}(\lambda_1 + \lambda_2)], \quad (22)$$

where λ_1 and λ_2 are restricted by the condition $\lambda_{\text{eff}} \geq 0$.

We finish this section by analyzing Eq. (21) at the special value of opening angle $\theta_0 = \pi/2$. At this value of θ_0 there is an essential difference in the z_1 behavior around $\tau = 0$ from that at other angles. If $\lambda_1 \neq \lambda_2$, then the leading behavior of z_1 is determined by the first-rank pole of

the coefficient of z_1 on the right-hand side of the equation. One of the solutions will have a logarithmic behavior around $\tau=0$ and the other one will map $\tau=0$ to $z_1=0$, both of them are physically unreasonable. So we must have $\lambda_1=\lambda_2$. Compensating the loss of one parameter, the two solutions of Eq. (21) with $\theta_0=\pi/2$ and $\lambda_1=\lambda_2$ both satisfy the requirement that $z_1(\tau)$ is real on $-1\leq\tau\leq 1$. The solutions therefore also form a family of two parameters. In fact, analytic solutions can be obtained in this case and have the form

$$z_1 = (1-\tau)^{(1-\lambda_1)/2} (1+\tau)^{(1+\lambda_1)/2} + c(1+\tau)^{(1-\lambda_1)/2} (1-\tau)^{(1+\lambda_1)/2}. \quad (23)$$

The solutions correspond to any real positive constant c and $0\leq\lambda_1\leq 1$. The solution found by Thome *et al.* [9] corresponds to the case $c=1$, which is the symmetric solution. Unfortunately, closed-form expression such as this can only be found when $\theta_0=\pi/2$.

III. SELECTIONS WITH SURFACE TENSION

As is now well known, in the linear channel geometry the inclusion of surface tension will break the continuous family of solutions into an infinite countable discrete set of solutions, and all the selected finger widths will go to a unique value as the surface tension approaches zero [5,6]. In the channel geometry, this value is equal to 0.5. Although there exist more rigorous methods of determining the selected finger width, the WKB method has proved much simpler.

Recently, BKLR [10] calculated the selected finger width at the small-surface-tension limit using a WKB

method in 90° geometry where a family of self-similar solutions were known. We start this section by briefly reviewing the WKB method.

As was noticed in the experimental paper [9], finite surface tension cannot be consistent with self-similar solutions. The paper suggested introducing a time-dependent injection rate. A more interesting suggestion was made in Ref. [10], where the authors consider a time-dependent surface tension $\gamma_{\text{phys}}=\gamma_0 t^{1/2}$. They argued that because one is only interested in the limit $\gamma_{\text{phys}}\rightarrow 0$, and because the changing rate of γ_0 will eventually become much smaller than any eigenvalues of the stability operator around the selected solutions, this assumption is valid for calculating the limiting value of selected finger width.

Assuming the deviation from the zero-surface-tension self-similar solution is $\delta(y)$, and linearizing the equation around the known zero-surface-tension solution $x_0(y)$, they obtain for $\delta(y)$

$$\frac{\gamma_0 \delta''(y)}{[1+x_0'(y)^2]^{3/2}} + L[x_0(y)]\delta(y) = \gamma_0 \kappa_0(y), \quad (24)$$

where L is some linear integral operator. The solvability condition is then

$$\int \kappa_0(y) \hat{\delta}_0(y) dy = 0, \quad (25)$$

where $\hat{\delta}_0(y)$ is the zero mode of the adjoint linear operator (Due to different coordinate system, our x (or y) coordinate is the y (or x) coordinate in Ref. [10]). Using a WKB ansatz and a local approximation of the integral operator L (readers are referred to Ref. [10], where this is shown in detail), $\hat{\delta}_0(y)$ is expressed

$$\hat{\delta}_0(y) \sim \exp \left[\frac{i}{\sqrt{\gamma_0}} \int_{x'(y)}^{x'(y)} \frac{(1-iz)^{3/4} (1+iz)^{1/4} [x_0(z) + iy_0(z)]^{1/2}}{g(z)} dz \right], \quad (26)$$

where $g(z) = d^2 x_0 / dy_0^2$ with $z = dx_0 / dy_0$.

It is easy to see that the integral (25) has a stationary phase point at $z = \pm i$. If one can deform the integral contour without crossing any singularity to the stationary-phase line passing through $z = i$, then the integral will be dominated by the contribution from the stationary-phase point and will never be zero, and therefore no selection is possible. From the expression for $\hat{\delta}_0(x)$, it is also obvious that the integrand of (25) will have a branch cut at point \bar{z} with $g(\bar{z})=0$. In the linear geometry, the zero point of $g(z)$ lies on the imaginary axis and is below the stationary point when the width of the finger is larger than 0.5. Because the branch cut passes through the stationary point, the contributions from left and right stationary path will have different phases and therefore can satisfy condition (25). That is the reason behind the fact that the finger width approaches 0.5 at small surface tension.

In the sector geometry, the distribution of the branch points is different. There are two branch points in the upper half plane distributed symmetrically around the imaginary axis. As the branch cut no longer passes

through the stationary phase point, for condition (25) to be satisfied, the contribution of the integral around the branch point has to be large enough to cancel the contribution from the stationary-phase point. The selected finger width at the small-surface-tension limit is then determined by

$$\text{Im} \int_z^i \frac{(1-iz)^{3/4} (1+iz)^{1/4} [x_0(z) + iy_0(z)]^{1/2}}{g(z)} dz = 0. \quad (27)$$

In Ref. [10], this calculation was done for the 90°-geometry case, and very good agreement was obtained between the theoretically derived selection width and that observed experimentally.

We now extend this derivation to a sector geometry of arbitrary angle using the results obtained in Sec. II. Because there is no asymmetric forcing in this problem, we assume the selected finger is symmetric around the center line of the sector [11], i.e., $\lambda_1=\lambda_2\equiv\lambda$.

Before extending the solution to the complex plane, we

would like to show how to obtain the interface shape from Eq. (21). We first make the transformation

$$z_1(\tau) = (1 - \tau^2)^{(1-\lambda)/2} z_2(\tau). \quad (28)$$

Then Eq. (21) becomes

$$\begin{aligned} \frac{d^2 z_2}{d\tau^2} + \left[\frac{2(\lambda-1)\tau}{1-\tau^2} + \frac{1-2\theta_0/\pi}{\tau} \right] \frac{dz_2}{d\tau} \\ = \frac{(\lambda-1)(1+\lambda-2\theta_0/\pi)}{1-\tau^2} z_2. \end{aligned} \quad (29)$$

Because the physical solution of this equation has to be even in τ , and because z_2 has to be real on $-1 \leq \tau \leq 1$, we have the boundary condition $z_2(1) = z_2(-1) = 1$ up to an unimportant constant.

Let us introduce a new variable φ : $\tau = \exp(i\varphi)$; the interface AOB corresponds to the segment on the real axis: $0 \leq \varphi \leq \pi$ [φ is related to ψ by $\varphi = \frac{1}{2}(\pi - \psi)$]. Solving the revised equation (29) with the boundary condition $z_2(\varphi=0) = z_2(\varphi=\pi)$, together with the transformation (12) and (28), we can obtain the interface parametrized by φ : $x_0(\varphi) = \text{Re}z(\varphi)$ and $y_0(\varphi) = \text{Im}z(\varphi)$ on $0 \leq \varphi \leq \pi$.

To extend the solution to the complex plane, we substitute all the transformations back to Eq. (10) and obtain a rather simple equation for $z(\varphi)$:

$$\frac{d^2 z}{d\varphi^2} = - \left[\left(\frac{\theta_0}{\pi} \right)^2 + \frac{1-\lambda^2}{4} \frac{1}{\sin^2 \varphi} \right] z. \quad (30)$$

The real and imaginary part of this equation can be extended from the real axis to the whole complex plane. The equations satisfied by $x(\varphi)$ and $y(\varphi)$, the complex

extension of x_0 and y_0 , are (we omit the subscript 0 from now on)

$$\frac{d^2 U}{d\varphi^2} = - \left[\left(\frac{\theta_0}{\pi} \right)^2 + \frac{1-\lambda^2}{4} \frac{1}{\sin^2 \varphi} \right] U, \quad (31)$$

where U can be x or y .

From Eq. (31), we can see that both $d^2 x/d\varphi^2$ and $d^2 y/d\varphi^2$ and therefore $d^2 x/dy^2$ are equal to zero when

$$\left(\frac{\theta_0}{\pi} \right)^2 + \frac{1-\lambda^2}{4} \frac{1}{\sin^2 \varphi} = 0, \quad (32)$$

i.e., when

$$\varphi = \pm i\alpha, \quad \pi \pm i\alpha, \quad \sinh(\alpha) = \frac{\pi}{2\theta_0} (1-\lambda^2)^{1/2}. \quad (33)$$

It is easy to show that $dx/dy|_{\varphi=\pm i\alpha} = -(dx/dy)|_{\varphi=\pi \pm i\alpha}$ *, so the branch points of the integral (25) are distributed symmetrically around the imaginary axis. We also know from numerical calculation that $\varphi = -i\alpha$ and $\pi - i\alpha$ correspond to the two branch points in the upper half plane.

It is convenient to calculate the integral of Eq. (27) in the φ plane. In order to do that, we have to find the point in φ plane that satisfied $dx/dy = \pm i$. Writing $\varphi = \pi/2 + i\varphi'$ with real φ' in Eq. (31) and using the conditions $dx/d\varphi|_{\varphi=\pi/2} = y|_{\varphi=\pi/2} = 0$, $y(\pi/2 + i\varphi')$ is pure imaginary $x(\pi + i\varphi')$ is pure real. So the solutions for $dx/dy = \pm i$ are $\varphi = \pi/2 \mp i\beta$, where $\beta (> 0)$ is a real number which can be obtained numerically. Now Eq. (25) becomes

$$\text{Im} \int_{\pi/2 - i\beta}^{-i\alpha} \left[1 + i \frac{dx/d\varphi}{dy/d\varphi} \right]^{3/4} \left[1 - i \frac{dx/d\varphi}{dy/d\varphi} \right]^{1/4} (x + iy)^{1/2} \frac{dy}{d\varphi} d\varphi = 0. \quad (34)$$

We integrate Eq. (31) from $(\pi/2, 0)$ to $(\pi/2, -\beta)$, and then from $(\pi/2, -\alpha)$ to $(0, -\alpha)$. Next we plug the result for x and y on the path $(0, -\alpha) \rightarrow (\pi/2, -\alpha) \rightarrow (\pi/2, -\beta)$ into the above integral to solve Eq. (34). The results of selected λ , defined as λ_s , for different opening angles are shown in Table I. The real finger width λ_{eff} is obtained according to the relation

$$\lambda_{\text{eff}} = 1 - \frac{\pi}{2\theta_0} (1 - \lambda). \quad (35)$$

The finger width determined by our calculation agrees with the experimental result within 5%. Even more strikingly, the selected λ value stays almost constant in the range $30^\circ \leq \theta_0 \leq 90^\circ$, $\lambda \approx 0.87$. Thus according to relation (35), λ_{eff} should have the behavior

$$\lambda_{\text{eff}} \approx 1 - 11.7^\circ / \theta_0. \quad (36)$$

Experimentally, the same behavior was observed in approximately the same range with the constant 10° instead of 11.7° as in our expression.

We also list the value of the real part of dx/dy at the

branch point: $\text{Re}z$ in Table I. We show in the table that the branch points approach the imaginary axis as the opening angle decreases.

Another interesting issue of the problem is the linear stability of the selected solutions. Experimentally, it was found that, at least for large opening angles, the finger pattern is unstable against tip splitting after some time (or at a certain distance from the origin). Theoretically, in channel geometry, it was demonstrated numerically [7] and later analytically [8] using the WKB method that the only stable solution is the one which has the lowest width, and the n th solution will have $n-1$ unstable modes. The analytical analysis by Bensimon, Pelce, and Shraiman in Ref. 8 was based on the local flatness of the interface compared with the capillary length and the use of the Mullins-Sekarka instability result. This analysis will certainly be applicable to the sector-geometry case, where the self-similar interface will become flatter as time increases. In addition, the validity of the WKB method in the sector geometry is proved by the accuracy of predicting the selected finger width, so the same result should be present in the sector geometry, i.e., the lowest

TABLE I. Various quantities (defined in the text) vs the opening angle.

θ_0	λ_s	λ_{eff}	$\text{Re}(\bar{z})$	$I(\lambda_s)$
0.175	0.952	0.572	0.175	0.028
0.248	0.937	0.602	0.214	0.031
0.322	0.923	0.624	0.248	0.052
0.395	0.911	0.646	0.280	0.072
0.468	0.901	0.668	0.319	0.092
0.542	0.892	0.686	0.374	0.113
0.615	0.884	0.705	0.418	0.135
0.689	0.879	0.724	0.459	0.155
0.762	0.874	0.741	0.496	0.194
0.836	0.870	0.756	0.543	0.211
0.909	0.869	0.773	0.577	0.246
0.983	0.867	0.787	0.619	0.283
1.056	0.863	0.796	0.656	0.327
1.130	0.861	0.807	0.694	0.367
1.203	0.859	0.816	0.747	0.394
1.277	0.856	0.822	0.794	0.444
1.350	0.856	0.832	0.838	0.488
1.424	0.856	0.842	0.885	0.533
1.497	0.858	0.851	0.934	0.581
1.571	0.861	0.861	0.980	0.647

branch of solutions are linearly stable.

The experiment is certainly in disagreement with the simple argument given above. We are going to remove this discrepancy by demonstrating the difference of the structure of the selected solutions in the sector geometry from that of the channel geometry. More explicitly, we are going to show that the lowest branch of solutions does not exist at small enough γ_0 [12]. As we showed before, the main contributions to the integral in (25) come from three parts, two from the path near the branch points $\varphi = -i\alpha$ and $\pi - i\alpha$ and one from the path around the stationary point $\varphi = -i\beta$. Neglecting all the slowly varying functions of γ_0 at small γ_0 , we can then write (25) approximately as

$$\exp\left[\frac{i\hat{\delta}(\varphi = -i\alpha)}{\sqrt{\gamma_0}}\right] + \exp\left[\frac{i\hat{\delta}(\varphi = \pi - i\alpha)}{\sqrt{\gamma_0}}\right] + \exp\left[\frac{i\hat{\delta}(\varphi = \pi/2 - i\beta)}{\sqrt{\gamma_0}}\right] = 0. \quad (37)$$

Let us define

$$R(\lambda) = -\text{Im}[\hat{\delta}(\varphi = -i\alpha) - \hat{\delta}(\varphi = \pi/2 - i\beta)],$$

$$I(\lambda) = \text{Re}[\hat{\delta}(\varphi = -i\alpha) - \hat{\delta}(\varphi = \pi/2 - i\beta)].$$

Because

$$\hat{\delta}(\varphi = -i\alpha) - \hat{\delta}(\varphi = \pi/2 - i\beta) = [\hat{\delta}(\varphi = \pi - i\alpha) - \hat{\delta}(\varphi = \pi/2 - i\beta)]^*,$$

we have

$$1 + \exp(R(\lambda)/\sqrt{\gamma_0})\cos[I(\lambda)/\sqrt{\gamma_0}] = 0. \quad (38)$$

As shown in Fig. 2, solutions of the above equation exist

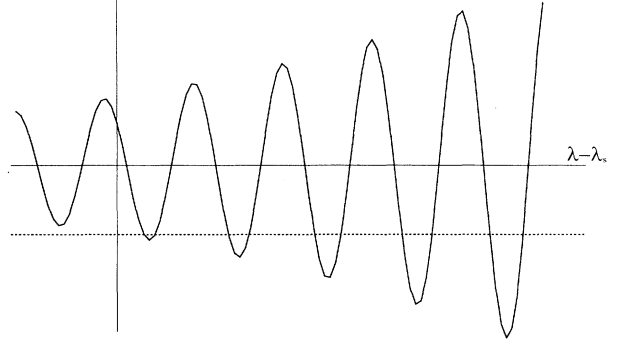


FIG. 2. Illustration of the solution of Eq. (38).

in the region with $R(\lambda) > 0$. The limit as $\gamma_0 \rightarrow 0$ on the selected value of λ , λ_s , is determined by the equation $R(\lambda_s) = 0$. We check the behavior of $I(\lambda)$ around $\lambda = \lambda_s$ and obtain numerically $I(\lambda_s) > 0$ and $dI/d\lambda|_{\lambda=\lambda_s} > 0$ for all angles. Because of this behavior of $I(\lambda)$, it is easy to see that as γ_0 decreases, the lowest and the second-lowest solutions will approach λ_s and eventually disappear as a pair; as γ_0 decreases even more, the third- and the fourth-lowest solutions will disappear as a pair, and so on.

We also list the value of $I(\lambda_s)$ in Table I. As we can see, $I(\lambda_s)$ goes to zero as the angle decreases to zero, which means that the solutions disappear at smaller γ_0 as we go to smaller angles. In fact, as is well known, the solutions never disappear at finite surface tension in the channel geometry.

Finally, we notice that for constant real surface tension γ_{phys} , γ_0 decreases with increasing time as $\gamma_0 = \gamma_{\text{phys}} t^{-1/2}$. Thus for real physical system where γ_{phys} is a constant, γ_0 will eventually decrease to the region where the only linearly stable solution is unavailable and the pattern will develop tip-splitting instability. For smaller opening angles, it will take a longer time for the tip-splitting instability to occur.

IV. SUMMARY

In the preceding sections, we have found an analytical method to find the self-similar solutions at zero surface tension. The solutions form a two-parameter family, exactly analogous to the two-parameter-family solutions found in channel geometry. In one special case $\theta_0 = \pi/2$, we get a closed form of the solution, and the solutions of Thome *et al.* are just the symmetric subset of our general solutions. We extend the WKB calculation of BKLR of the 90° geometry to arbitrary opening angles, and excellent agreement with experiment is reached in the whole range of opening angles. We also demonstrated that the selected solutions will disappear in pairs due to the structure of the branch points and stationary point in the complex plane. Based on this result and the fact that the effective surface tension decreases with increasing time, we are able to explain the instability found in experiment.

Note added. After finishing this work, we learned that analytical solutions were also found by M. Benamar in a different coordinate system for the same geometry. Her one-parameter family of solutions is the same as the set of symmetric solutions in our paper, i.e., for the case where $\lambda_1 = \lambda_2$.

ACKNOWLEDGMENTS

The author would like to thank Professor H. Levine and W. Rappel for many helpful discussions and careful reading of the manuscript. This work was supported in part by the U.S. Defense Advanced Projects Administration under the University Research Initiative, Grant No. N00014-86-K-0758.

APPENDIX: THE CONVERGENT-GEOMETRY CASE

In Ref. [9], an experiment was also done in the convergent geometry (see Fig. 3), where the finger approaches the origin. The zero-surface-tension solutions can be found in exactly the same fashion as in Sec. II (the divergent case).

We look for self-similar solutions of the form (5). Because the finger approaches the origin as time increases, we have

$$h(t) \frac{dh(t)}{dt} = -1, \quad h(t) = \sqrt{2(t_0 - t)}, \quad (\text{A1})$$

where t_0 is the final time when the interface touches the origin.

The problem is now reduced to finding an analytical function $z(\omega)$ in the negative infinite strip $-\pi \leq \psi \leq \pi$, $-\infty < \psi \leq 0$, with the boundary conditions (i) $\arg(z) = \pm \theta_0/2$ on $\psi = \pm \pi$, (ii) $z \sim \exp(\omega \theta_0/2\pi)$ when $\phi \rightarrow -\infty$, and (iii) z satisfies $\text{Im}(z^* \partial z / \partial \psi) = -1$ on $\phi = 0$.

By going through exactly the same analysis discussed in detail in Sec. II, and making the transformations

$$z = \exp(\theta_0 \omega / 2\pi) z_1, \\ \tau = (-\exp \omega)^{1/2},$$

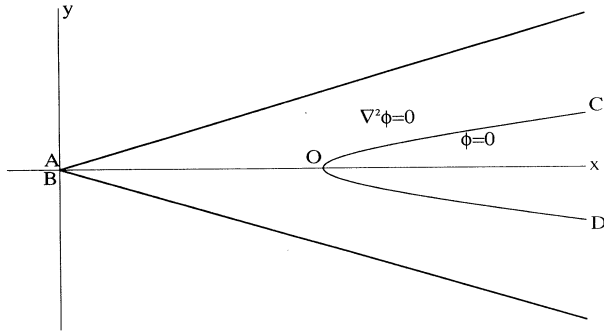


FIG. 3. Illustration of the convergent case.

we have

$$\frac{d^2 z_1}{d\tau^2} + \frac{1 + 2\theta_0/\pi}{\tau} \frac{dz_1}{d\tau} \\ = \frac{1}{\tau(\tau^2 - 1)^2} \left[\left(\frac{\lambda_1^2 + \lambda_2^2}{2} - 1 \right) \tau + \frac{\lambda_1^2 - \lambda_2^2}{4} (\tau^2 + 1) \right]. \quad (\text{A2})$$

We choose the solution $z_1^{(1)}$, which is finite at $\tau = 0$.

Due to the condition that $z_1 \rightarrow \infty$ as $\tau \rightarrow \pm 1$, the parameters λ_1 and λ_2 have to be greater than 1: $\lambda_{1(2)} \geq 1$. The relative angular width λ_{eff} of the finger with respect to the opening angle is

$$\lambda_{\text{eff}} = 1 + \frac{\pi}{2\theta_0} \left[1 - \frac{1}{2}(\lambda_1 + \lambda_2) \right], \quad (\text{A3})$$

where λ_1 and λ_2 are restricted by the condition $\lambda_{\text{eff}} \geq 0$.

When we compare the main results here [Eqs. (A2) and (A3)] from that of Sec. II [Eqs. (21) and (22)], we can see that they are the same if we make the change $\theta_0 \rightarrow -\theta_0$. Following the experimental paper, we therefore identify the convergent case as the negative θ_0 case of Sec. II.

As in the convergent case, when $\theta_0 = \pi/2$, we can find the closed form of the symmetric solutions:

$$z_1 = (\tau^{-1} - 1)^{(1-\lambda_1)/2} (1 + \tau^{-1})^{(1+\lambda_1)/2} \\ - (1 + \tau^{-1})^{(1-\lambda_1)/2} (\tau^{-1} - 1)^{(1+\lambda_1)/2} \quad (\text{A4})$$

with $1 \leq \lambda_1 \leq 2$. The reason that we cannot obtain closed-form asymmetric solutions such as Eq. (23) is that z_1 has to be finite as τ goes to zero.

In order to use the WKB method, we have to find the zero point of $d^2 x / dy^2$ (we only consider the symmetric case $\lambda_1 = \lambda_2 \equiv \lambda$ here, just as in the divergent case.). Changing τ to $\tau = \exp i\varphi$, it is easy to see that the interface solution can be extended to the complex plane by using the same equations as in the divergent case: Eq. (31). The zero point of $d^2 x / dy^2$ is therefore determined by

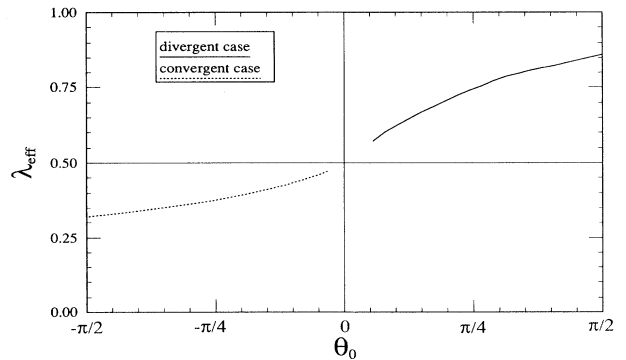


FIG. 4. Angular width of the selected finger vs the opening angle.

$$\left(\frac{\theta_0}{\pi}\right)^2 + \frac{1-\lambda^2}{4} \frac{1}{\sin^2\varphi} = 0. \quad (\text{A5})$$

Because λ is defined in different range from that in the divergent case, we discuss the solutions of the above equation in two regions: (i) $1 \leq \lambda \leq [1 + (2\theta_0/\pi)^2]^{1/2}$; here the solutions of Eq. (A5) are $\varphi = \alpha$ and $\pi - \alpha$, where $\sin\alpha = (\pi/2\theta_0)(\lambda^2 - 1)^{1/2}$. This corresponds to the case where the tip region of the pattern has negative curvature. (ii) $[1 + (2\theta_0/\pi)^2]^{1/2} \leq \lambda \leq 1 + 2\theta_0/\pi$; here the solutions of Eq. (A5) are $\varphi = \pi/2 \pm i\alpha$, where $\cosh\alpha = (\pi/2\theta_0)(\lambda^2 - 1)^{1/2}$.

The solutions in region (i) correspond to real dx/dy and according to the analysis in Sec. III, the solutions in

region (ii) correspond to pure imaginary dx/dy . So as λ increases, the branch points of integral (25) in the dx/dy plane will approach and eventually exceed the stationary point $dx/dy = \pm i$. The critical value of λ is determined by the condition that the branch point coincides with the stationary point, just as in the linear channel case. The resulting λ_{eff} is plotted against the opening angle in Fig. 4, together with the results from the divergent case.

The results agree with experiment with $\theta_0 \geq -40^\circ$. It differs from experiment beyond this range, where only two data points were shown in Ref. [9] ($\theta_0 = -60^\circ$ and -90°). Finally, we have to point out here that the validity of the WKB method in this case is not justified because we have assumed a time-varying surface tension, $\gamma_0 = \gamma_{\text{phys}}(t_0 - t)^{-1/2}$, which increases with time.

-
- [1] For a general review of interfacial pattern formation, see D. Kessler, J. Koplik, and H. Levine, *Adv. Phys.* **37**, 255 (1988); J. S. Langer, in *Chance and Matter*, edited by J. Souletie (North-Holland, Amsterdam, 1987).
- [2] For more details about the Saffman-Taylor problem, see D. Bensimon, L. Kadanoff, S. Liang, B. I. Shraiman, and L. Tang, *Rev. Mod. Phys.* **58**, 977 (1986); G. M. Homsy, *Annu. Rev. Fluid Mech.* **19**, 271 (1987).
- [3] P. G. Saffman and G. I. Taylor, *Proc. R. Soc. London Ser. A* **245**, 312 (1958). The two parameter family of solutions were found in a later paper: G. I. Taylor and P. G. Saffman, *Q. J. App. Mech. Appl. Math.* **12**, 265 (1959).
- [4] D. Kessler, J. Koplik, and H. Levine, *Phys. Rev. A* **31**, 1712 (1985); E. Ben-Jacob, N. Goldenfeld, G. Kotliar, and J. S. Langer, *Phys. Rev. Lett.* **53**, 2110 (1984).
- [5] J. M. Mclean and P. G. Saffman, *J. Fluid Mech.* **102**, 455 (1981); L. Romero, Ph.D. thesis, California Institute of Technology, 1982; J. M. Vanden-Broeck, *Phys. Fluids* **26**, 8 (1983).
- [6] B. I. Shraiman, *Phys. Rev. Lett.* **56**, 2028 (1986); D. Hong and J. S. Langer, *ibid.* **56**, 2032 (1986); R. Combescot, T. Dombre, V. Hakim, Y. Pomeau, and A. Pumir, *ibid.* **56**, 2036 (1986); *Phys. Rev. A* **37**, 1270 (1988); S. Tanveer, *Phys. Fluids* **30**, 1589 (1987).
- [7] D. Kessler and H. Levine, *Phys. Rev. A* **33**, 2621 (1986); **33**, 2634 (1986); D. Kessler and H. Levine, *Phys. Fluids* **30**, 1246 (1987).
- [8] D. Bensimon, P. Pelce, and B. I. Shraiman, *J. Phys. Fluids* **48**, 2081 (1987).
- [9] H. Thome, M. Rabaud, V. Hakim, and Y. Couder, *Phys. Fluids A* **1**, 224 (1989).
- [10] E. Berner, D. Kessler, H. Levine, and W. Rappel, *Europhys. Lett.* **13** (2), 161 (1990).
- [11] The nonsymmetric patterns can be selected when there exists asymmetric forcing in the problem. For some detail, see, E. Berner, H. Levine, and Y. Tu, *Phys. Fluids A* **3**, 529 (1991).
- [12] The nonexistence of the lowest branch of solutions at small surface tension was observed in numerical calculation by M. Ben-Amar (private communication); a qualitative explanation was given by V. Hakim, which is essentially the same as the one we discuss here.